Journal of Zhejiang University-SCIENCE A in press
www.jzus.zju.edu.cn; www.springer.com/journal/11582
E-mail: jzus_a@zju.edu.cn

Research Article
https://doi.org/10.1631/jzus.A2500172

Fixed-time robust attitude tracking control for high-speed aircraft: a precise funnel-guided approach

Kai AN, Wei HUANG✉, Shuangxi LIU
Advanced Propulsion Technology Laboratory, National University of Defense Technology, Changsha 410073, China

Abstract: In this article, we present a robust fixed-time attitude control scheme with severe funnel driving constraints for high-speed aircraft developed concerning uncertain signals. Firstly, an adaptive fixed-time radial basis function neural network (AFTR) observer is described, designed as a compensation control based on a converted attitude error system, aiming at eliminating the influence of strong disturbances and uncertainties. Then, we propose a performance-prescribed transformation strategy that can effectively enhance the accuracy of error tracking and state convergence by constructing second-order performance error functions. Based on the above preparation and transformation, we present a double-integral fixed-time sliding mode controller combined with an auxiliary oscillation-suppression function designed to achieve fixed-time convergence of attitude angles and angular rates, which ensures the rapidity of error tracking and state convergence. Finally, the fixed-time stability of the entire closed-loop system is proved via Lyapunov synthesis theory, and the upbound of convergence time is derived. Nominal and comparative simulation cases were used to investigate the effectiveness and reliability of the proposed integrated framework.

Key words: Funnel control; Fixed-time theory; Attitude control; RBFNN; High-speed aircraft

Unedited

1 Introduction

High performance attitude control has a profound effect on the success of unmanned vehicle missions, such as the learning control of quadruped robots (Shao et al., 2024), the navigation, guidance, and control of unmanned aerial vehicles (Chen et al., 2024), the path tracking of a sailboat (Shao et al., 2024), and the orbiting entry, landing and sample return of the Chang'e lunar exploration program (Liu et al., 2021). It crucial for high-speed aircraft systems with complex dynamic coupled characteristics and environmental constraints to have a rapid signal response and anti-disturbance capability. The techniques of performance-prescribed control (PPC), fixed-time control (FTC), and radial basis function neural networks (RBFNN) have emerged as prominent research fields.

✉ Wei HUANG, gladrain2001@163.com
Wei HUANG, https://orcid.org/0000-0001-9805-985X

Received May 8, 2025; Revision accepted Sept. 16, 2025; Crosschecked

© Zhejiang University Press 2025

PPC was originally introduced by Bechlioulis and Rovithakis (2008) with the objective of obtaining predetermined steady-state and transient performance. The effective performance function is the essential feature that differentiates the PPC from other control approaches. Furthermore, the design of the performance function has an immediate impact on the final simulation results. Due to its shape, the performance function is also referred to as the funnel function (Berger and Rauert, 2020). Many performance functions integrated with different control methodologies have been developed for high-speed aircraft. Bu (2023) developed a performance function independent of initial state errors by combining it with an exponential function for longitudinal fuzzy control, which enhances the flexibility of boundary adjustment. A boundary-adjustable prescribed performance controller combined with a back-stepping technique was proposed by Wang and Hu (2018) to address the perturbation and saturation issues of a sudden system crash. This was further improved by Bu et al. (2023), Song and Zhang (2024) and Lun et al. (2024) to tolerate sudden error fluctuation. Some scholars also

demonstrated the advantages of PPC by integrating performance functions with control methods like dynamic surface control (Yin et al., 2024) and output feedback control (Li et al., 2023). With the development of intelligent approaches, Xu et al. (2022) extended the finite-time performance function proposed by Tan and Guo (2022) to the attitude control of high-speed aircraft and proposed a fixed-time control scheme based on a reinforcement learning module. Zhao et al. (2023a) developed a hybrid intelligent controller considering prescribed performance constraints and a critic-only adaptive dynamic programming approach. However, these methods have some reliability issues. A typical problem is that the tracking state errors approach boundaries and repeat high-frequency oscillations, which seriously compromises system stability. In addition, a sufficient convergence space (i.e., large steady-state error range) may sacrifice transition performance and cause unstable transient histories of errors. As a complementary transformation measurement, the PPC scheme needs to be combined with other control methods to realize its performance advantages.

In view of its advantages, fixed-time theory (Polyakov, 2012) can be introduced into the PPC framework to provide accurate system control. Fixed-time convergence establishes stricter theoretical limitations than asymptotic and finite-time control methods. It requires an analytically explicit expression for the upper bound constraint of convergence time, which enables the overall convergence time of the system to be controllable through parameter modification. Fixed-time theory combined with sliding mode control has been widely applied to high-speed aircraft (Parsegov et al., 2012; Zuo and Tie, 2014), and shows that the fixed settling time can be estimated for any initial states. Wu et al. (2021) designed a quantized double-loop fixed-time fault-tolerant attitude controller with a fixed-time extended state observer to ensure overall control performance. Similarly, Dong et al. (2022) developed a fixed-time fuzzy adaptive fault-tolerant control methodology. Chen et al. (2023) designed a double-integral fixed-time sliding mode manifold and fixed-time controller to avoid the decoupling problem of complex attitude variation of high-speed morphing aircraft. Zhang et al. (2024b) further developed a fixed-time flight control strategy based on homogenous system theory. Furthermore, an event-triggered mechanism was introduced into a specific fixed-time control theory proposed by Moulay et al. (2022) to maintain the robustness of the attitude system and reduce the control updating frequency (Zhang et al., 2023). Zhao et al. (2022) designed a fixed-time attitude control scheme combined with the back-stepping technique. In addition to integration with conventional control approaches, intelligent learning is increasingly expanding the range of applications for fixed-time theory, such as the finite-time deterministic learning control framework proposed by Guo and Xu (2022), barrier Lyapunov function-based predefined time learning control (Wang et al. 2024) and intelligent fault diagnosis-based fixed-time learning control scheme (Wang and Xia, 2024). Overall, the fixed-time theory has the capability to stabilize state errors rapidly, but there is still an extensive requirement to respond to strong coupled high-speed aircraft systems and further enhance the research exploration of applications.

With the appropriate parameters, PPC and fixed-time theory can effectively drive the tracking errors to arbitrarily small values if the system is not influenced by uncertain signals. However, it is necessary to introduce a compensation observer to estimate the external disturbances and propagated uncertainties within the system, which may potentially make the system diverge (Bouaiss et al., 2024). As an intelligent approximation method, the RBFNN can effectively address the trade-off between function complexity and approximation accuracy through its inherent neural network capabilities. This method has already been extensively explored in model approximation (Bao et al., 2023), parameter estimation (Shen et al., 2023); (Zhang et al., 2024), and disturbance prediction (Zhao and Yang, 2022; Zhao et al., 2023) in high-speed aircraft systems. But RBF networks generally fail to meet the requirements for convergence speed and are unable to rapidly predict system disturbances based on dynamic responses. The fixed-time control theory emphasizes guaranteed convergence speed of the system, which ensures that the system can reach a steady-state convergence region within a predefined upper bound of time, expressed in explicit analytical form. This

Unedited

avoids potential instability issues (Ding et al., 2022; Sun et al., 2020), ensuring swift estimation of disturbances. By leveraging the fitting capability of RBFNN and the fixed-time convergence guaranteed by fixed-time adaptive laws, developing a composite disturbance observer will effectively achieve a feasible trade-off between estimation accuracy and convergence speed. Meng et al. (2024) developed a fixed-time RBFNN disturbance observer and derived a fitting error expression for reusable launch vehicles. Li et al. (2024) designed a fixed-time disturbance observer for inertia uncertainties in attitude tracking control of spacecraft. Thus, it is imperative to design a secure observer by combining RBFNN with fixed-time theory for potential disturbance. A complete summary of adaptive updating law design and detailed system analysis for the complicated and coupled angle/angular rate system will be outlined.

Motivated by the above discussion and based on the preceding research foundation of sliding mode control (An et al., 2022), the integrated attitude-tracking control approach was further developed for a generic high-speed model within a disturbed flight environment. The main contributions of this article are as follows:

- Faced with the weakness of wide boundaries of steady-state error and uncontrollable error trajectories of existing PPC approaches applied in attitude control (Bu, 2023; Bu et al., 2023; Bu and Xiao, 2018; Li et al., 2023; Lun et al., 2024; Song and Zhang, 2024; Wang and Hu, 2018; Yin et al., 2024), a funnel-guided PPC scheme combined with improved funnel boundaries is proposed to eliminate the unexpected transition history, reach narrow steady-state error thresholds, and achieve rapid error convergence.
- Compared with the existing fixed-time sliding mode controllers of Chen et al. (2023), an effective double-integral fixed-time sliding mode manifold is proposed to guarantee stable and rapid convergence of the attitude angles and angular rates. To eliminate asymptotic oscillation in the tracking process, an auxiliary oscillation-suppression function is designed simultaneously, which has been proven to have a good effect.
- To address the significant effects of uncertain signals, a fixed-time RBFNN enhancement observer with a developed adaptive weight updating law named AFTR is designed to eliminate unknown disturbances and uncertainties from the dynamic model, atmosphere parameters, and perturbation factors in both attitude angle and angular rate channels.

The rest of this article is organized as follows: Section II introduces the approach with some preliminary notes and lemmas, and describes the problem formulation. Section III provides the main results, including the AFTR enhancement observer, funnel-guided PPC, fixed-time sliding mode tracking controller, and parameter tuning guideline, together with corresponding demonstrations of stability. Finally, numerical simulations are presented in Section IV.

2 Preliminaries and problem formulation

2.1 Preliminaries

LEMMA 1 (Chen et al., 2021). Assume there is a continuous positive definite and radially unbounded function $\mathcal{V}(x)$ with state x such that $\dot{\mathcal{V}}(x) \leq -\mathcal{K}_1\mathcal{V}^{p_1}(x) - \mathcal{K}_2\mathcal{V}^{q_1}(x) + \xi$, where $\mathcal{K}_1, \mathcal{K}_2 > 0$, and satisfying $0 < p_1 < 1$, $q_1 > 1$, where ξ denotes a small positive constant. `The system will converge to the origin x_0 in fixed-time equilibrium with settling time $\mathcal{T}_1(x_0)$ bounded by

$$\mathcal{T}_1(x_0) \leq \mathcal{T}_{1,\max} = \frac{1}{\mathcal{K}_1\delta(1-p_1)} + \frac{1}{\mathcal{K}_2\delta(q_1-1)}$$

The residual set Q of the system is given as follows, with constant $0 < \delta < 1$, where $\min\{\cdot\}$ represents the minimum value:

$$Q = \left\{ x | \mathcal{V}(x) \leq \min\left\{ \left[\frac{\xi}{\mathcal{K}_1(1-\delta)}\right]^{\frac{1}{p_1}}, \left[\frac{\xi}{\mathcal{K}_2(1-\delta)}\right]^{\frac{1}{q_1}} \right\} \right\}$$

LEMMA 2 (Xin et al., 2023). According to Corollary 1, for a continuous Lyapunov function like $\dot{\mathcal{V}}(x) \leq -\mathcal{K}_1\mathcal{V}^{\frac{q_1}{q_2}}(x) - \mathcal{K}_2\mathcal{V}^{\frac{q_1}{q_2}}(x) - \mathcal{K}_3\mathcal{V}(x) + \epsilon$, where $\mathcal{K}_1$, $\mathcal{K}_2$, $\mathcal{K}_3 > 0$, $0 < \epsilon < \infty$, α_1, α_2, β_1, β_2 are all positive odd numbers, and $\alpha_1 > \alpha_2, \beta_1 < \beta_2$, then the system $\dot{x} = f(x,t)$, $x(0) = 0$ is semiglobal practical fixed-time stability (SPFS), in which the fixed convergence time $\mathcal{T}_2$ is given by

Unedited

$$\mathcal{T}_2 \le \mathcal{T}_{2,\max} = \max\left\{\frac{\alpha_2 \ln(1+\frac{\mathcal{K}_3}{\delta\mathcal{K}_1})}{\mathcal{K}_3(\alpha_1-\alpha_2)}, \frac{\alpha_2 \ln(1+\frac{\delta\mathcal{K}_3}{\mathcal{K}_1})}{\delta\mathcal{K}_3(\alpha_1-\alpha_2)}\right\} + \max\left\{\frac{\beta_2 \ln(1+\frac{\mathcal{K}_3}{\delta\mathcal{K}_2})}{\mathcal{K}_3(\beta_2-\beta_1)}, \frac{\beta_2 \ln(1+\frac{\delta\mathcal{K}_3}{\mathcal{K}_2})}{\delta\mathcal{K}_3(\beta_2-\beta_1)}\right\}$$

where $\max\{\cdot\}$ represents the maximum value, $0 < \delta < 1$ and the residual set Q with output $\mathcal{Y}(x)$ of the system is expressed as

$$Q = \left\{x | \mathcal{Y}(x) \le \min\left\{\left[\frac{\epsilon}{\mathcal{K}_1(1-\delta)}\right]^{\frac{\alpha_2}{\alpha_1}}, \left[\frac{\epsilon}{\mathcal{K}_2(1-\delta)}\right]^{\frac{\beta_2}{\beta_1}}, \frac{\epsilon}{\mathcal{K}_3(1-\delta)}\right\}\right\}$$

LEMMA 3 (Zuo, 2015). For $x_i \in \mathbb{R}^+ (i = 1, ..., n)$:

$$\sum_{i=1}^{n} |x_i|^{\chi} \ge \begin{cases} (\sum_{i=1}^{n} |x_i|)^{\chi}, 0 < \chi \le 1 \\ n^{1-\chi}(\sum_{i=1}^{n} |x_i|)^{\chi}, \chi > 1 \end{cases}$$

LEMMA 4 (Qian and Lin, 2001). For the constants $\mathcal{K}_1 > 1$, $\mathcal{K}_2 > 1$, the equation $\frac{1}{\mathcal{K}_1} + \frac{1}{\mathcal{K}_2} = 1$ holds, then the following expression is established:

$$|xy| \le \frac{\epsilon^{\mathcal{K}_1}}{\mathcal{K}_1}|x|^{\mathcal{K}_1} + \frac{1}{\mathcal{K}_2 \epsilon^{\mathcal{K}_2}}|y|^{\mathcal{K}_2}$$

for arbitrary $x \in \mathbb{R}$, $y \in \mathbb{R}$ and $\epsilon > 0$.

2.2 Dynamics modeling and problem description

The differential attitude subsystem with angle of attack α, sideslip angle β and bank angle μ as tracking states is as follows:

$$\begin{cases} \dot{\alpha} = q - \tan\beta(p\cos\alpha + r\sin\alpha) + \frac{-L+\overline{G}_\alpha+\overline{F}_{d\alpha}}{m_0 V\cos\beta} \\ \dot{\beta} = p\sin\alpha - r\cos\alpha + \frac{Y+\overline{G}_\beta+\overline{F}_{d\beta}}{m_0 V} \\ \dot{\mu} = \frac{p\cos\alpha + r\sin\alpha}{\cos\beta} + \frac{\overline{G}_\mu+\overline{F}_{d\mu}}{m_0 V} + \frac{L(\tan\beta+\tan\gamma\sin\mu)+Y\tan\gamma\cos\mu}{m_0 V} \end{cases} \quad (1)$$

where q, r and p represent the angular rates of pitch, yaw, and roll, respectively, m_0 is the mass, V is the velocity, and γ is the flight path angle. $\overline{F}_d = \left[\overline{F}_{d\alpha}, \overline{F}_{d\beta}, \overline{F}_{d\mu}\right]^{\mathrm{T}}$ are the aerodynamic disturbance force components acting on three channels. $\overline{G} = \left[\overline{G}_\alpha, \overline{G}_\beta, \overline{G}_\mu\right]^{\mathrm{T}}$ represents the equivalent components of gravity in the three control channels. The detailed expression of $\overline{G}$ is given in Section S2.2 Eq. (1) of the Electronic Supplementary Materials.

The angular rate subsystem is described as

$$\begin{cases} \dot{q} = \frac{J_x - J_x}{J_y} pr + \frac{M_m + x_{cg}(D\sin\alpha + L\cos\alpha) + \Delta M_Y}{J_y} \\ \dot{r} = \frac{J_x - J_y}{J_z} pq + \frac{M_n - x_{cg}Y + \Delta M_Z}{J_z} \\ \dot{p} = \frac{J_y - J_z}{J_x} qr + \frac{M_l + \Delta M_X}{J_x} \end{cases} \quad (2)$$

where the lift force L, drag force D and side force Y can be written as $L = C_L\overline{q}S$, $D = C_D\overline{q}S$ and $Y = C_Y\overline{q}S$, and the force moments for three axes are $M_l = C_l\overline{q}bS$, $M_m = C_m\overline{q}cS$, and $M_n = C_n\overline{q}bS$. C_L, C_D, C_Y, C_l, C_m, C_n are the aerodynamic coefficients, b is the wingspan and c is the mean aerodynamic chord. The dynamic pressure is calculated by $\overline{q} = \frac{1}{2}\overline{\rho}V^2$ with atmospheric density $\overline{\rho}$. S is the surface area of the vehicle, x_{cg} is the center of gravity, and the uncertain moment vector is expressed by $\Delta M = [\Delta M_Y, \Delta M_Z, \Delta M_X]^{\mathrm{T}}$. $\boldsymbol{J} = \mathrm{diag}\{J_y, J_z, J_x\}$ represents the moment of inertia.

The above two subsystems can be simplified as a general nonlinear vector expression:

$$\begin{aligned} \dot{\boldsymbol{\Omega}} &= \boldsymbol{g}_\Omega \boldsymbol{\omega} + \Delta_\Omega \\ \dot{\boldsymbol{\omega}} &= \boldsymbol{f}_\omega + (\boldsymbol{g}_\omega + \Delta\boldsymbol{g}_\omega)\boldsymbol{u} + \Delta_{\omega f} \end{aligned} \quad (3)$$

where $\boldsymbol{\Omega} = [\alpha, \beta, \mu]^{\mathrm{T}}$, $\boldsymbol{\omega} = [q, r, p]^{\mathrm{T}}$, and $\boldsymbol{u} = [\delta_{\mathrm{e}}, \delta_{\mathrm{a}}, \delta_{\mathrm{r}}]^{\mathrm{T}}$ is the control input.

The terms $\Delta_\Omega = \frac{1}{m_0 V}\left[\frac{\overline{F}_{d\alpha}}{\cos\beta}, \overline{F}_{d\beta}, \overline{F}_{d\mu}\right]^{\mathrm{T}}$ and $\Delta_{\omega f} = \left[\frac{\Delta M_Y}{J_y}, \frac{\Delta M_Z}{J_z}, \frac{\Delta M_X}{J_x}\right]^{\mathrm{T}}$ are caused by unknown disturbances and uncertain components. $\Delta\boldsymbol{g}_\omega$ represents the model uncertainties due to aerodynamic perturbation and atmospheric error. The specific expressions for some notations in Eq. (3) are given in Section S2.2 Eqs. (2)-(3) of the Electronic Supplementary Materials. Let $\boldsymbol{f}_\omega = \left[f_q, f_r, f_p\right]^{\mathrm{T}}$, and the detailed expressions are given in Section S2.2 Eq. (4) of the Electronic Supplementary Materials.

The angle reference command is denoted as $\boldsymbol{\Omega}_d(t_0)$ in initial time t_0. To ensure the smooth continuity of the reference signals and protect the control quantity from excessive sudden change and fluctuations, a first-order filter is introduced into the signal interface. Then the filtered input signal in the next discretized time point t_1 is obtained by

$$\overline{\boldsymbol{\Omega}}_d(t_1) = k_{ft}\boldsymbol{\Omega}_d(t_0) + (1 - k_{ft})\overline{\boldsymbol{\Omega}}_d(t_0) \quad (4)$$

where k_{ft} is the filter coefficient and $\overline{\boldsymbol{\Omega}}_d$ is the filtered guidance command.

The following control-oriented second-order

Unedited

error dynamic model Eq. (5) is then developed as follows, based on the attitude model Eq. (3). This model aims to convert the original state errors to assist the construction of subsequent dual-channel fixed-time controllers.

$$\begin{aligned}\dot{\boldsymbol{e}}_\Omega &= \dot{\boldsymbol{\Omega}} - \dot{\overline{\boldsymbol{\Omega}}}_d = \boldsymbol{g}_\Omega \boldsymbol{\omega} - \dot{\overline{\boldsymbol{\Omega}}}_d + \Delta_\Omega \\ \dot{\boldsymbol{e}}_\omega &= \dot{\boldsymbol{\omega}} - \dot{\boldsymbol{\omega}}_d = \boldsymbol{f}_\omega + \boldsymbol{g}_\omega \boldsymbol{u} - \dot{\boldsymbol{\omega}}_d + \Delta_\omega\end{aligned} \tag{5}$$

where $\boldsymbol{\omega_d}$ represents the reference angular rate, which can be obtained by the angular subsystem through the backstepping method, and $\boldsymbol{\Delta_\omega} = \boldsymbol{\Delta g_\omega u} + \boldsymbol{\Delta_{\omega f}}$.

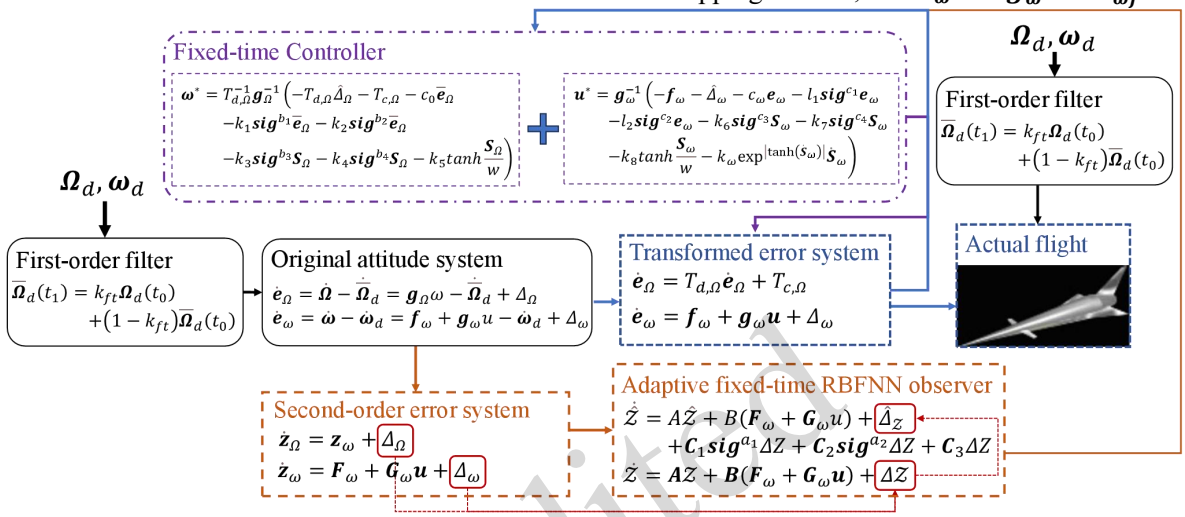

Fig. 1: Integrated fixed-time control framework.

Based on the above dynamic models and relevant parameters, the main purpose of this study was to develop a funnel-guided fixed-time controller (FGFTC) with an AFTR observer to address the following issues:

1. Estimate the unknown comprehensive uncertainties Δ_Ω and Δ_ω composed of aerodynamic perturbation, external disturbances and atmospheric uncertainties precisely, then derive the fixed-time convergence characteristics with the designed AFTR observer.
2. With the given initial state conditions and guided performance-prescribed funnel, the attitude angle error vector $\boldsymbol{e}_\Omega$ and the angular rate error vector $\boldsymbol{e}_\omega$ can achieve a fast convergence to the equilibrium points of the control system in fixed time.

3 Main results

First, we introduce an observer design to address inherent uncertainties in nonlinear systems (Eq. (3)) and external disturbances. Then, a fixed-time robust controller for an attitude closed-loop system is presented, featuring a performance-prescribed funnel shrinking guidance for transforming error dynamics. Meanwhile, an auxiliary oscillation-suppressing measure is implemented in the proposed controller to facilitate rapid oscillation elimination. The integrated fixed-time control framework developed in this study is illustrated in Fig. 1, and the detailed design procedure is provided below.

3.1. AFTR enhancement observer

Considering the nonlinear system Eq. (3), define error vectors $\boldsymbol{z}_\Omega = \boldsymbol{\Omega} - \overline{\boldsymbol{\Omega}}_d, \boldsymbol{z}_\omega = \boldsymbol{g}_\Omega\boldsymbol{\omega} - \dot{\overline{\boldsymbol{\Omega}}}_d$, then the system can be rewritten as

$$\begin{aligned}\dot{\boldsymbol{z}}_\Omega &= \boldsymbol{z}_\omega + \Delta_\Omega \\ \dot{\boldsymbol{z}}_\omega &= \boldsymbol{F}_\omega + \boldsymbol{G}_\omega\boldsymbol{u} + \Delta_\omega\end{aligned} \tag{6}$$

where $\boldsymbol{F}_\omega = \dot{\boldsymbol{g}}_\Omega\boldsymbol{\omega} + \boldsymbol{g}_\Omega\boldsymbol{f}_\omega - \dot{\overline{\boldsymbol{\Omega}}}_d$, $\boldsymbol{G}_\omega = \boldsymbol{g}_\Omega\boldsymbol{g}_\omega$, $\Delta_\omega = \boldsymbol{g}_\Omega(\Delta\boldsymbol{g}_\omega\boldsymbol{u} + \Delta_\omega\boldsymbol{f}_\omega)$. The term $\dot{\overline{\boldsymbol{\Omega}}}_d$ can be easily obtained under the assumption that the reference signal is second-order differentiable.

Define a combined vector $\mathcal{Z} = \left[\boldsymbol{z}_\Omega^{\mathrm{T}}, \boldsymbol{z}_\omega^{\mathrm{T}}\right]^{\mathrm{T}}$, then the second-order nonlinear system Eq. (6) is rewritten as the compound form

$$\dot{\mathcal{Z}} = \boldsymbol{A}\mathcal{Z} + \boldsymbol{B}(\boldsymbol{F}_\omega + \boldsymbol{G}_\omega\boldsymbol{u}) + \Delta\mathcal{Z} \tag{7}$$

where $\boldsymbol{A} = \begin{bmatrix}\boldsymbol{0}_{3\times3} & \boldsymbol{1}_{3\times3} \\ \boldsymbol{0}_{3\times3} & \boldsymbol{0}_{3\times3}\end{bmatrix}$, $\boldsymbol{B} = [\boldsymbol{0}_{1\times3}, \boldsymbol{1}_{1\times3}]^{\mathrm{T}}$, $\Delta\mathcal{Z} = \left[\Delta_\Omega^{\mathrm{T}}, \Delta_\omega^{\mathrm{T}}\right]^{\mathrm{T}}$, $\boldsymbol{0}$ represents a vector with all zeros, $\boldsymbol{1}$ denotes the vector of all ones.

Before the detailed observer error analysis, the designed AFTR observer is first given as

Unedited

$$\dot{\widehat{\mathcal{Z}}} = \boldsymbol{A}\widehat{\mathcal{Z}} + \boldsymbol{B}(\boldsymbol{F}_\omega + \boldsymbol{G}_\omega \boldsymbol{u}) + \widehat{\Delta}_{\mathcal{Z}} + \boldsymbol{C}_1 \boldsymbol{sig}^{a_1} \Delta\mathcal{Z} + \boldsymbol{C}_2 \boldsymbol{sig}^{a_2} \Delta\mathcal{Z} + \boldsymbol{C}_3 \Delta\mathcal{Z} \tag{8}$$

where $\widehat{\mathcal{Z}}$ is the observed state vector and $\widehat{\Delta}_{\mathcal{Z}}$ is the estimated value of comprehensive disturbances and uncertainties for $\widehat{\mathcal{Z}}$. $\Delta\mathcal{Z} = \mathcal{Z} - \widehat{\mathcal{Z}}$ denotes the observation error, and $a_1 \in (0,1)$, $a_2 = 2 - a_1$. Based on the discussion, the term $\widehat{\Delta}_{\mathcal{Z}}$ is approximated by RBFNN.

Based on the general neural network expression from Section S3.1 Eqs. (5)-(6) from the Electronic Supplementary Materials, the real and estimated disturbance terms $\Delta_{\mathcal{Z}}$ *and* $\widehat{\Delta}_{\mathcal{Z}}$ can be similarly defined by

$$\Delta_{\mathcal{Z}} = \boldsymbol{W}^T h(\mathcal{Z}) + \epsilon(\mathcal{Z}) \qquad \widehat{\Delta}_{\mathcal{Z}} = \widehat{\boldsymbol{W}}^T h(\mathcal{Z}) \tag{9}$$

where $\boldsymbol{W}$, $\widehat{\boldsymbol{W}} \in \mathbb{R}^{N\times 6}$ are the optimal and approximated weight vectors individually, and the corresponding estimated weight errors can be given by

$$\widetilde{\boldsymbol{W}} = \boldsymbol{W} - \widehat{\boldsymbol{W}} \tag{10}$$

Assumption 1 (Chen et al., 2023). The NN approximation error $\epsilon(\cdot)$ has the upper bound ϵ_N satisfying $\| \epsilon(\cdot) \| \leq \epsilon_N$ and the ideal weights are assumed to be bounded as $\| \boldsymbol{W} \| \leq W_N$.

Subscribing Eq. (7) and Eq. (8) into $\Delta\mathcal{Z}$, the following dynamics can be derived:

$$\Delta\dot{\mathcal{Z}} = \boldsymbol{A}\Delta\mathcal{Z} + \widetilde{\boldsymbol{W}}^T h(\mathcal{Z}) + \epsilon(\mathcal{Z}) - \boldsymbol{C}_1 \boldsymbol{sig}^{a_1} \Delta\mathcal{Z} - \boldsymbol{C}_2 \boldsymbol{sig}^{a_2} \Delta\mathcal{Z} - \boldsymbol{C}_3 \Delta\mathcal{Z} \tag{11}$$

where $\boldsymbol{C}_1, \boldsymbol{C}_2$ are both diagonal matrices and the diagonal elements $c_{1,i}, c_{2,i} > 0$, $\boldsymbol{C}_3 = \begin{bmatrix} \boldsymbol{0}_{3\times3} & \boldsymbol{D}_{3\times3} \\ \boldsymbol{0}_{3\times3} & \boldsymbol{0}_{3\times3} \end{bmatrix}$, where $\boldsymbol{D}_{3\times3} = \mathrm{diag}\{d_n\}$, $n = 1,2,3$, $d_n > 1$. The function $\boldsymbol{sig}^l \boldsymbol{x} = \mathrm{sgn}(\boldsymbol{x}) \|\boldsymbol{x}\|^l$ and $\mathrm{sgn}(\boldsymbol{x})$ represents the sign of $\mathbf{x}$.

Then, the following convergence theorem of the observer is described and proved.

Theorem 1. The proposed AFTR adaptive enhancement observer (Eq. (8)) can guarantee that the observation error (Eq. (11)) converges to a neighborhood of origin in a fixed time with the NN adaptive weight updating law $\widehat{\boldsymbol{W}} = \boldsymbol{P} h \Delta\mathcal{Z}^{\mathrm{T}} - \widehat{\boldsymbol{W}}$. The detailed proof process can be found in Section S3.1 of the Electronic Supplementary Materials.

Remark 1. Theorem 1 shows that the condition $\| \widetilde{\boldsymbol{W}} \| \approx 0$ can be satisfied when the system time satisfies $T_s > T_{0,\max}$, meaning that the observation error $\widetilde{\Delta}_{\mathcal{Z}}$ will converge to zero in the fixed time T_s with the Assumption 1, respectively. Thus, it is reasonable to assume that the state errors $\widetilde{\Delta}_\Omega, \widetilde{\Delta}_\omega$ have the upper bounds satisfying $\| \widetilde{\Delta}_\Omega \| \leq D_\Omega$ and $\| \widetilde{\Delta}_\omega \| \leq D_\omega$ when the convergence time $T_0 > T_s$, respectively. Meanwhile, it can be further assumed that the derivatives $\dot{\widetilde{\Delta}}_\Omega, \dot{\widetilde{\Delta}}_\omega$ exist and are continuously bounded satisfying $\| \dot{\widetilde{\Delta}}_\Omega \| \leq D_\Omega$, $\| \dot{\widetilde{\Delta}}_\omega \| \leq D_\omega$.

3.2. Funnel-guided prescribed performance methodology

In general, the metrics of control performance are expressed by steady-state error, transition history, and settling time. Unrestricted states may lead to uncontrollable transitional convergence histories and invalid control signals over a prolonged period. The performance-prescribed technique sets strict boundaries for error states during the entire convergence phase, ensuring that tracking errors can remain within certain intervals to meet performance requirements.

The tracking errors of angle states expressed by Eq. (5) are constrained by the designed boundaries named funnel functions, which can be introduced by $-\rho_{\mathcal{L}}(t) \leq e_i(t) \leq \rho_{\mathcal{U}}(t)$, $i = \alpha, \beta, \mu$, where $\rho_{\mathcal{L}}(t)$ and $\rho_{\mathcal{U}}(t)$ are the lowbound and upbound functions. The smooth funnel functions $\rho_{\mathcal{L}}(t)$, $\rho_{\mathcal{U}}(t)$ must satisfy two requirements: 1) $\rho_{\mathcal{L}}(t)$, $\rho_{\mathcal{U}}(t) > 0$ are continuously differentiable functions, and $\lim_{t\to\infty} \rho_j(t) = \rho_{j\infty}$, $j = \mathcal{L}, \mathcal{U}$, $\rho_{j,\infty}$ is the steady-state error boundary; 2) The derivative of the funnel function is semi-negative definite. The traditional exponential funnel function of Bechlioulis and Rovithakis (2008) and some improved funnel functions (Bu, 2023; Bu et al., 2023; Bu and Xiao, 2018; Li et al., 2023; Lun et al., 2024; Song and Zhang, 2024; Wang and Hu, 2018; Yin et al., 2024) still show some conflicts in terms of generality while being effectively applied to solve their relevant scientific challenges: 1° wide steady-state error boundaries; 2° uncontrollable error trajectories. This section is focused mainly on shrinking the steady-state error range and accelerating the convergence of error trajectories.

Taking the challenge term 1° into account, we present an improved funnel function that has stable transition performance and adjustable steady-state

Unedited

error boundaries. The proposed funnel function is defined as follows:

$$\begin{aligned}\rho(t) &= \rho_0/\cosh(lt)\\ \rho_{\mathcal{L}}(t) &= -\operatorname{sgn}(e_i(0))\tanh\left(\frac{e_i(0)}{a_\rho}\right)\rho(t) - \rho_{i,\infty}\\ \rho_{\mathcal{U}}(t) &= \operatorname{sgn}(e_i(0))\tanh\left(\frac{e_i(0)}{a_\rho}\right)\rho(t) + \rho_{i,\infty}\end{aligned} \tag{12}$$

where ρ_0 is the initial boundary, l is a constant determining the convergence speed of the performance-prescribed boundary, $e_i(0)$ is the initial error of state i, $\rho_{i,\infty}$ denotes the ultimate steady-state error of state i, and a_ρ is a constant satisfying $a_\rho \in (0,1)$. Because of the properties of the hyperbolic tangent function, a_ρ should be appropriately provided in the simulation for an effective steady-state error history range.

Remark 2. The hyperbolic tangent function, denoted as $\tanh(\cdot)$, serves as an adaptive variable constraint term to limit the initial error. This function has two main features: 1) it can indirectly indicate the positivity or negativity of the original state error; 2) it can adaptively enlarge or reduce the constraint boundaries. Finally, the tracking errors will converge to predefined steady-state values with gradually shrinking performance limitations.

Considering the second challenge 2°, a funnel-guided error transition strategy is proposed to lead the error convergence trajectory. Define an auxiliary variable $s_{i,e} = e_i - e_{i,\mathrm{op}}$, $i = \alpha, \beta, \mu$, $e_{i,\mathrm{op}} = k_s\rho_{\mathcal{L}} + (1-k_s)\rho_{\mathcal{U}}$ and $k_s \in (0,1)$, then the derivative of $s_{i,e}$ is given by $\dot{s}_{i,e} = \dot{e}_i - \dot{e}_{i,\mathrm{op}}$. Then the range of $s_{i,e}$ is simultaneously transformed into $s_{\mathcal{L}}(t) \le s_{i,e}(t) \le s_{\mathcal{U}}(t)$, $s_{\mathcal{L}}(t) = \rho_{\mathcal{L}}(t) - e_{i,\mathrm{op}}$ and $s_{\mathcal{U}}(t) = \rho_{\mathcal{U}}(t) - e_{i,op}$.

To convert the auxiliary error variable into the unconstrained space, the following transformation function is defined:

$$\begin{aligned}\bar{e}(t) &= \ln\left(\frac{\zeta(t)}{1-\zeta(t)}\right)\\ \zeta(t) &= \frac{s_{i,e}(t)-s_{\mathcal{L}}(t)}{s_{\mathcal{U}}(t)-s_{\mathcal{L}}(t)}\end{aligned} \tag{13}$$

Then the transformed error equation can be derived by Eq. (14), where the terms T_d and T_c are described in Section S3.2 Eq. (14) of the Electronic Supplementary Materials.

$$\begin{aligned}\dot{\bar{e}}(t) &= \frac{\dot{\zeta}(t)}{\zeta(t)}\left(1+\frac{\zeta(t)}{1-\zeta(t)}\right)\\ &= \frac{(s_{\mathcal{U}}-s_{\mathcal{L}})}{(s_{i,e}-s_{\mathcal{L}})(s_{\mathcal{U}}-s_{i,e})}\dot{s}_{i,e}\\ &\quad + \frac{s_{i,e}(\dot{s}_{\mathcal{L}}-\dot{s}_{\mathcal{U}})-\dot{s}_{\mathcal{L}}s_{\mathcal{U}}+\dot{s}_{\mathcal{U}}s_{\mathcal{L}}}{(s_{i,e}-s_{\mathcal{L}})(s_{\mathcal{U}}-s_{i,e})}\\ &= T_d\dot{s}_{i,e} + T_c\end{aligned} \tag{14}$$

Remark 3. Note that if $s_{i,e} \to 0$, the state error e_i will converge to $e_{i,\mathrm{op}}$. The coefficient k_s is crucial to control error convergence trajectories, which will influence the transient performance of e_i and significantly enhance the controllability and stability during the error convergence process. Based on the above discussion, the performance-prescribed transformation method in this article is called the funnel-guided convergence strategy.

Remark 4. Some singularity issues will occur in Eq. (13). This is manifested mainly in the following aspects: firstly, the large convergence speed with the small steady-state boundary of the funnel boundary is infeasible. In this case, the controller in the angular velocity loop cannot respond rapidly to changes in the reference angular rate, resulting in the accumulation of angle errors and causing the error value to exceed the funnel boundary. Secondly, an improper value of k_s will lead to a significant discrepancy between the actual initial angle error and the reference value. In this case, the controller in the angular velocity loop will deviate from the reference angular rate command during the initial period, resulting in the accumulation of angle errors and causing the error value to exceed the funnel boundary. Therefore, it is necessary to coordinate the relationship between the funnel boundary convergence speed, the steady-state error boundary, the reference error trajectory, and the dynamic characteristics of the angular rate loop based on the parameter tuning guideline in Section 3.5 to effectively avoid singularity issues in Eq. (13).

Based on the designed funnel function Eq. (12) and transformed guidance strategy Eq. (14), the error dynamics of the attitude angle loop in Eq. (5) is further rewritten as the following expression, and the angular rate loop holds:

$$\begin{aligned}\dot{\boldsymbol{e}}_{\boldsymbol{\Omega}} &= \boldsymbol{T}_{d,\boldsymbol{\Omega}}\dot{\boldsymbol{e}}_{\boldsymbol{\Omega}} + \boldsymbol{T}_{c,\boldsymbol{\Omega}}\\ \dot{\boldsymbol{e}}_{\boldsymbol{\omega}} &= \boldsymbol{f}_{\boldsymbol{\omega}} - \dot{\boldsymbol{\omega}}_{\boldsymbol{d}} + \boldsymbol{g}_{\boldsymbol{\omega}}\boldsymbol{u} + \boldsymbol{\Delta}_{\boldsymbol{\omega}}\end{aligned} \tag{15}$$

where $T_{d,\Omega}$ and $T_{c,\Omega}$ are described in Section S3.2 Eq. (15) of the Electronic Supplementary Materials.

Remark 5. In this article, only the angle states are

Unedited

transformed into the performance-prescribed constraints, and the angular rates will maintain convergence characteristics by the following fixed-time angular controller for two reasons. First, the stable angle error trajectories can provide high-quality input signals for angular rates to minimize the divergence risk, and second, the strict-limitation angular rates will complicate parameter tuning and system structure, which may worsen the controller oscillation frequency and is not practical for real-world applications.

3.3. Fixed-time attitude tracking controller design

Based on the proposed AFTR and performance-prescribed methodology, a fixed-time attitude tracking control scheme was developed to ensure strong stability of the entire closed-loop flight control system.

For the attitude angle control subsystem, considering the transformed state error $\bar{\boldsymbol{e}}_\Omega = \left[\bar{e}_\alpha, \bar{e}_\beta, \bar{e}_\mu\right]^{\mathrm{T}} \in \mathbb{R}^3$, the double-integral sliding mode manifold $\boldsymbol{S}_\Omega$ is constructed by

$$\boldsymbol{S}_\Omega = \bar{\boldsymbol{e}}_\Omega + c_0 \int_0^t \bar{\boldsymbol{e}}_\Omega \,\mathrm{d}\tau + \int_0^t k_1 \boldsymbol{sig}^{b_1} \bar{\boldsymbol{e}}_\Omega + k_2 \boldsymbol{sig}^{b_2} \bar{\boldsymbol{e}}_\Omega \mathrm{d}\tau \quad (16)$$

where c_0, k_1, k_2, b_1, b_2 are all constants, and $b_1 > 1$, $0 < b_2 < 1$.

A desired virtual angular rate controller $\boldsymbol{\omega}^*$ can be designed as

$$\begin{aligned}\boldsymbol{\omega}^* = T_{d,\Omega}^{-1} \boldsymbol{g}_\Omega^{-1} (& - T_{d,\Omega} \widehat{\Delta}_\Omega - T_{c,\Omega} - c_0 \bar{\boldsymbol{e}}_\Omega \\ & - k_1 \boldsymbol{sig}^{b_1} \bar{\boldsymbol{e}}_\Omega - k_2 \boldsymbol{sig}^{b_2} \bar{\boldsymbol{e}}_\Omega \\ & - k_3 \boldsymbol{sig}^{b_3} \boldsymbol{S}_\Omega - k_4 \boldsymbol{sig}^{b_4} \boldsymbol{S}_\Omega - k_5 \tanh \frac{\boldsymbol{S}_\Omega}{w})\end{aligned} \quad (17)$$

where k_3, k_4, $k_5 > 0$, $b_3 > 1$, $0 < b_4 < 1$, $w > 0$.

The two integral terms of the proposed sliding mode manifold $\boldsymbol{S}_\Omega$ can ensure that output can closely match a small steady-state error. Yet, such a treatment may potentially destabilize and slow down the dynamic response of a closed-loop system. Further simulation tests reveal that ensuring the dynamic response at the convergence stage by tuning parameters alone is challenging. Therefore, to improve the dynamic transition characteristics of the system, an ancillary control term $\boldsymbol{u}_{\mathrm{comp}}$ is designed to compensate the controller Eq. (17) as follows:

$$\begin{aligned}\boldsymbol{\omega}^* = T_{d,\Omega}^{-1} \boldsymbol{g}_\Omega^{-1} (& - T_{d,\Omega} \widehat{\Delta}_\Omega - T_{c,\Omega} - c_0 \bar{\boldsymbol{e}}_\Omega \\ & - k_1 \boldsymbol{sig}^{b_1} \bar{\boldsymbol{e}}_\Omega - k_2 \boldsymbol{sig}^{b_2} \bar{\boldsymbol{e}}_\Omega \\ & - k_3 \boldsymbol{sig}^{b_3} \boldsymbol{S}_\Omega - k_4 \boldsymbol{sig}^{b_4} \boldsymbol{S}_\Omega - k_5 \tanh \frac{\boldsymbol{S}_\Omega}{w} \\ & + \boldsymbol{u}_{\mathrm{comp}})\end{aligned} \quad (18)$$

where

$$\boldsymbol{u}_{\mathrm{comp}} = - k_\Omega \exp^{|\tanh(\dot{\boldsymbol{S}}_\Omega)|} \frac{\mathrm{d}\boldsymbol{S}_\Omega(t)}{\mathrm{d}t} \quad (19)$$

where the constant $k_\Omega > 0$ and the coefficient $\mathcal{K}_\Omega = k_\Omega \exp^{|\tanh(\dot{\boldsymbol{S}}_\Omega)|}$ has the parameter range of $\mathcal{K}_\Omega \in (k_\Omega, 2.718 k_\Omega)$. The term $\frac{\mathrm{d}\boldsymbol{S}_\Omega(t)}{\mathrm{d}t}$ can initially be approximated by the following equation and the explanation can be found in Section S3.3 Eqs. (16)-(17) of the Electronic Supplementary Materials.

$$\dot{\boldsymbol{S}}_\Omega(t_0) = \frac{\mathrm{d}\boldsymbol{S}_\Omega(t_0)}{\mathrm{d}t} \approx \frac{\boldsymbol{S}_\Omega(t_0 + h_s) - \boldsymbol{S}_\Omega(t_0)}{h_s} \quad (20)$$

Lemma 5. Considering the designed virtual angle controller Eq. (18), the constructed sliding mode manifold $\boldsymbol{S}_\Omega$ will be fixed-time stable with analytical settling time T_Ω. The detailed proof process can be found in Section S3.3 of the Electronic Supplementary Materials.

For the attitude angular rate subsystem, the angular rate errors are denoted as $\boldsymbol{e}_\omega = \left[e_q, e_r, e_p\right]^{\mathrm{T}} \in \mathbb{R}^3$. Similar to Eq. (16), the angular rate sliding mode manifold $\boldsymbol{S}_\omega$ is given by

$$\boldsymbol{S}_\omega = \boldsymbol{e}_\omega + c_\omega \int_0^t \boldsymbol{e}_\omega \,\mathrm{d}\tau + \int_0^t l_1 \boldsymbol{sig}^{c_1} \boldsymbol{e}_\omega + l_2 \boldsymbol{sig}^{c_2} \boldsymbol{e}_\omega \mathrm{d}\tau \quad (21)$$

where the coefficients c_ω,l_1,$l_2 > 0$, $c_1 > 1$, $0 < c_2 < 1$. The derivative of $\boldsymbol{S}_\omega$ with respect to time t is

$$\dot{\boldsymbol{S}}_\omega = \boldsymbol{f}_\omega + \boldsymbol{g}_\omega \boldsymbol{u} + \Delta_\omega + c_\omega \boldsymbol{e}_\omega + l_1 \boldsymbol{sig}^{c_1} \boldsymbol{e}_\omega + l_2 \boldsymbol{sig}^{c_2} \boldsymbol{e}_\omega \quad (22)$$

Then the designed actual control input $\boldsymbol{u}^*$ is given by

$$\begin{aligned}\boldsymbol{u}^* = \boldsymbol{g}_\omega^{-1} (& - \boldsymbol{f}_\omega - \widehat{\Delta}_\omega - c_\omega \boldsymbol{e}_\omega - l_1 \boldsymbol{sig}^{c_1} \boldsymbol{e}_\omega \\ & - l_2 \boldsymbol{sig}^{c_2} \boldsymbol{e}_\omega - k_6 \boldsymbol{sig}^{c_3} \boldsymbol{S}_\omega - k_7 \boldsymbol{sig}^{c_4} \boldsymbol{S}_\omega \\ & - k_8 \tanh \frac{\boldsymbol{S}_\omega}{w} - k_\omega \exp^{|\tanh(\dot{\boldsymbol{S}}_\omega)|} \dot{\boldsymbol{S}}_\omega)\end{aligned} \quad (23)$$

where k_6,k_7,k_8,$k_\omega > 0$, $c_3 > 1$, $0 < c_4 < 1$ and the coefficients $\mathcal{K}_\omega = k_\omega \exp^{|\tanh(\dot{\boldsymbol{S}}_\omega)|}$ satisfy $\mathcal{K}_\omega \in (k_\omega, 2.718 k_\omega)$.

Lemma 6. Considering the designed real controller Eq. (23), the constructed sliding mode manifold $\boldsymbol{S}_\omega$ will be fixed-time stable with analytical settling time T_ω. The detailed proof process is similar to that of Lemma 5 and can also be found in Section S3.3 of the Electronic Supplementary Materials.

3.4. Integrated stability analysis and discussion

In summary, the sliding mode motion can be divided into two stages: 1) first, the sliding mode variables $\boldsymbol{S}_\Omega$ and $\boldsymbol{S}_\omega$ converge to sliding mode hyperplanes ($\boldsymbol{S}_\Omega \to 0, \boldsymbol{S}_\omega \to 0$) from arbitrary initial states of the system; 2) second, the system states reach the equilibrium points ($\boldsymbol{e}_\Omega \to 0, \boldsymbol{e}_\omega \to 0$) along the hyperplanes. Having obtained the fixed-time

Unedited

convergence properties of the first stage from Lemmas 5 and 6, the stability analysis of the second stage is discussed in this section.

Theorem 2. Consider the transformed attitude error system Eq. (15), with the arbitrary initial conditions given. If the sliding mode surfaces $\boldsymbol{S}_{\Omega}$ and $\boldsymbol{S}_{\omega}$ converge to the effective residual sets, then the proposed AFTR observer Eq. (8) with weight updating law $\widehat{\boldsymbol{W}}$ and controllers Eq. (18), Eq. (23) with suitable parameters can guarantee that the observation errors $\tilde{\Delta}_{\Omega}$, $\tilde{\Delta}_{\omega}$ and the state errors $\bar{\boldsymbol{e}}_{\Omega}$, $\boldsymbol{e}_{\omega}$ can achieve a fast convergence to the equilibrium points in fixed time. Furthermore, the defined auxiliary state s_e can also converge to the original points, which means that the attitude angle error $\boldsymbol{e}_{\Omega}$ will converge to the reference trajectory $\boldsymbol{e}_{\mathrm{op}}$ in the fixed time, i.e., the fixed-time tracking control results of actual attitude angles can be obtained. The complete proof process can be found in Section S3.4 of the Electronic Supplementary Materials.

3.5. Parameter tuning guideline

Despite the relationship among some parameters, there is still a lack of guidance on how to fine-tune the main parameters so that the proposed observers and controllers can achieve the desired control performance. This section provides parameter-tuning tips for the AFTR, funnel boundaries, and fixed-time controllers. Meanwhile, the trade-off of convergence velocity and steady-state error range must be balanced simultaneously for the highly nonlinear system of high-speed aircraft. The control inputs are sensitive to a number of controller parameters from the funnel function depicted in Eq. (12) and the controllers illustrated in Eq. (18) and Eq. (23), which may lead to the accumulation of errors and delays during the convergence process.

Firstly, to enable the funnel boundary to guide error convergence behavior, an effective initial threshold ρ_0 needs to be provided, generally not less than the maximum initial state error. Then a feasible parameter factor k_s is required, which indicates the final steady-state error. A rapid convergence trajectory needs a large shrinking rate l , which significantly adjusts the convergence speed of the prescribed performance boundary. The shrinking rate can be selected from the range $l \in [0.5, 3]$ in this paper. Further, $\rho_{l,\infty}$ defines the final steady-state error boundary of angle state i, and the order of magnitude is less than 10^{-2} in this article. Except for the above crucial parameters, the convergence process of the state error is not sensitive to other PPC parameters.

Secondly, in the fixed-time controller, the exponents of fixed-time convergence terms, denoted as $b_1, b_2, b_3, b_4, c_1, c_2, c_3, c_4$, need to be determined appropriately according to Lemma 1 and Lemma 2. Generally, $b_1, b_3, c_1, c_3 > 1$ and $b_2, b_4, c_2, c_4 \in (0,1)$. The parameters b_1, b_3, c_1, c_3 need to be carefully selected, and the effective value is not greater than 5 in this article. After that, the control coefficients l_1, l_2 and k_j(j=1, 2 ,…, 8) can be set to 1 and then modified according to the system's behavior. Regarding the second integral terms in sliding mode manifolds Eq. (16) and Eq. (21), the coefficients k_1, k_2 and l_1, l_2 should be much smaller than the coefficients k_3, k_4, k_5, k_6, k_7, k_8 in main control terms. To reduce the effort needed to tune these control coefficients, similar terms can have the same coefficient settings between Eqs. (18) and (23) in the initial consideration. Further, the coefficients k_{Ω} and k_{ω} of the ancillary control terms should not be greater than 0.1.

With respect to the AFTR observer, the parameter design principle incorporates the following components:

- The numerical approximation capability of the neural network is directly influenced by the selection of m_j. Following the design principle of the Gaussian basis function, the approximation of input signals x_i can be enhanced by increasing the number of centroids of m_j and decreasing the Euclidean distance between m_j and x_i with nonlinear selection methods such as the Gaussian distribution.
- The variable n_j represents the bandwidth of the Gaussian basis function, which determines the mapping capability of the NN to state inputs. Typically, the parameter should satisfy the range $n_j \geq 1$.

Remark 6: Table 1 systematically summarizes all generic parameters and their corresponding values used in the controllers presented in this study. It not only provides typical empirical ranges of these parameters (derived from a comprehensive review and synthesis of related literature), but also specifies the actual values adopted in the simulation cases in

Unedited

accordance with these recommended ranges. This clarifies the connection between parameter guidance ranges and the specific values chosen for numerical simulations.

Table 1. The empirical range of parameter tuning

Modules	Parameters	Empirical range	Simulation value
Funnel module	ρ_0, k_s, l, $\rho_{i,\inf}$, a_ρ	$\rho_0 > e_0$, $k_s \in [0,1]$, $l > 0$, $\rho_{i,\inf} > 0$, $a_\rho \in (0,1)$	$\rho_0 > e_{i,0}$, $i = \alpha, \beta, \mu$ $k_s = 0.6$, $l \in [0.5,3]$, $\rho_{i,\inf} = 0.01$, $a_\rho = 10^{-4}$
AFTR observer	$\mathcal{N}$, $\boldsymbol{P}$, a_1, $c_{1,i}$ $c_{2,i}$, d_n	$\mathcal{N} > 0$, $a_1 \in (0,1)$, $c_{1,i} > 0$, $c_{2,i} > 0$, $d_n > 1$, $p_{1,i} > 0$, $p_{i,i} \in \boldsymbol{P}$	$\mathcal{N} = 500$, $a_1 = 0.5$, $c_{1,i} = c_{2,i} = 1$, $d_n = 1.5$, $\boldsymbol{P} = \mathrm{diag}\{4,4,4,1,1,1\}$
Angle tracking subsystem	c_0, b_1, b_2, k_1, k_2, b_3, b_4, k_3, k_4, k_5, w, k_Ω	$c_0 > 0$, $b_1, b_3 > 1$, $0 < b_2, b_4 < 1$, $w > 0$, $k_1 \sim k_5 > 0$, $k_\Omega > 0$	$0 < k_\Omega < 0.1$, $c_0 = 0.02$, $b_1 = 1.5$, $b_2 = 0.6$, $b_3 = 5$, $b_4 = 0.8$, $k_1 = 2 \times 10^{-5}$, $k_2 = 3 \times 10^{-5}$, $k_3 = 0.5$, $k_4 = 0.001$, $k_5 = 0.03$, $w = 1$
Angular rate tracking subsystem	c_ω, l_1, l_2, c_1, c_2, k_6, k_7, k_8, c_3, c_4, k_ω	$c_\omega > 0$, $c_1, c_3 > 1$, $0 < l_1, l_2 < 1$, $0 < c_2, c_4 < 1$, $k_6 \sim k_8 > 0$, $k_\omega > 0$	$0 < k_\omega < 0.1$, $c_\omega = 3$, $l_1 = 2 \times 10^{-5}$, $l_2 = 3 \times 10^{-5}$, $c_1 = 1.6$, $c_2 = 0.8$, $c_3 = 2$, $c_4 = 0.2$, $k_6 = 3$, $k_7 = 0.015$, $k_8 = 0.03$

Unedited

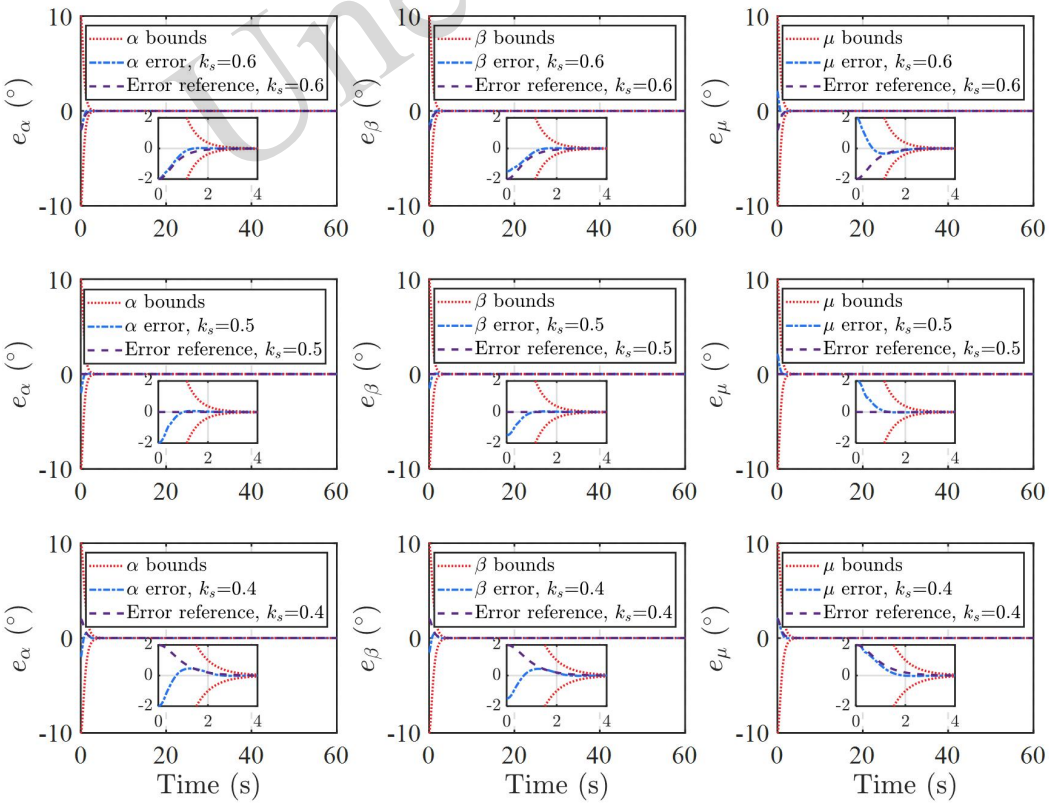

Fig. 2: The error convergence trajectories of attitude angles follow the reference trajectories obtained under the different control coefficient k_s.

4 Simulation verification

In this section, we describe the validation and comparative analysis of the proposed observer and controller. The first subsection focuses on the feasibility verification of the proposed attitude-integrated controller with the AFTR observer. The subsequent subsection evaluates control methods from the literature and highlights the reliability and robustness of the proposed framework.

The initial flight states of a winged-cone high-speed aircraft were given as $H = 33.5$ km, $V = 2590$ m/s, $\alpha = -2^{\circ}$, $\beta = -1.5^{\circ}$, $\mu = -0.43^{\circ}$, and other initial states were all set to zero. The parameters associated with the different modules integrated in the attitude tracking control system are summarized in Table.1. Some matrix parameters were as follows: the initial weights of the RBFNN are given by $\boldsymbol{W}_0 = \mathbf{0}_{N\times 1}$, the coefficients are $\{C_1, C_2, ..., C_j, ..., C_N\} \in \{-0.05, -0.0498, ..., 0, ..., 0.05\}$.

The following cases are discussed.

4.1. Nominal Cases

Along with the designed parameters, three validation scenarios were executed in this subsection.

1) Performance Verification with the Original PPC (Bechlioulis and Rovithakis, 2008) and the FGFTC: In this case, a comparative validation was performed to highlight the advantages of the proposed FGFTC. The tracking error results with the proposed performance guidance strategy are shown in Fig. 2, which compares the convergence trajectories in three-channel angle errors with different control factors $k_s = 0.4, 0.5, 0.6$, respectively. The results indicate that the angle errors can rapidly and accurately track the reference trajectories and achieve convergence without extra transition behaviors. Additionally, the overall convergence time of the angle subsystem is determined by the slowest convergence angle, and the close coupling among the three-channel parameters may delay the convergence speed.

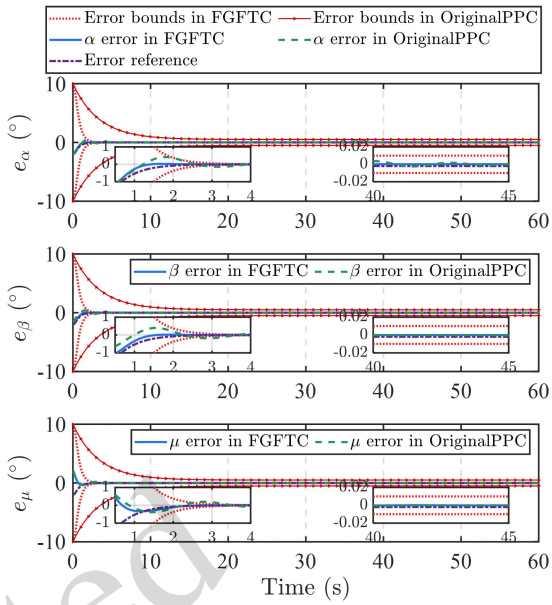

Fig. 3: Tracking errors and bounds of attitude angles compared with original PPC methods.

The advantages and robustness of the proposed strategy compared to the traditional PPC of Bechlioulis and Rovithakis (2008) are illustrated in Fig. 3. The most apparent advantage is the tight steady-state error range and the superiority of convergence speed, indicating that the angle errors can rapidly converge while remaining stable along with the reference error trajectories. We also conclude that the angle errors in FGFTC can reach $\mathbf{10^{-2}}$ orders of magnitude, yet the original PPC method cannot achieve this target. Fig. 3 shows the maximum achievable convergence speed and minimum steady-state error range of the original PPC method. Obviously, there is a gap between the original PPC and the method presented in this article.

Unedited

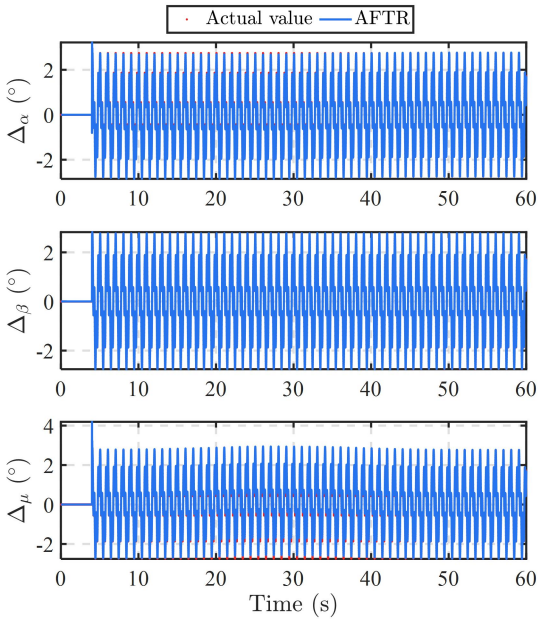

Fig. 4: Disturbance approximation in the attitude angle channel.

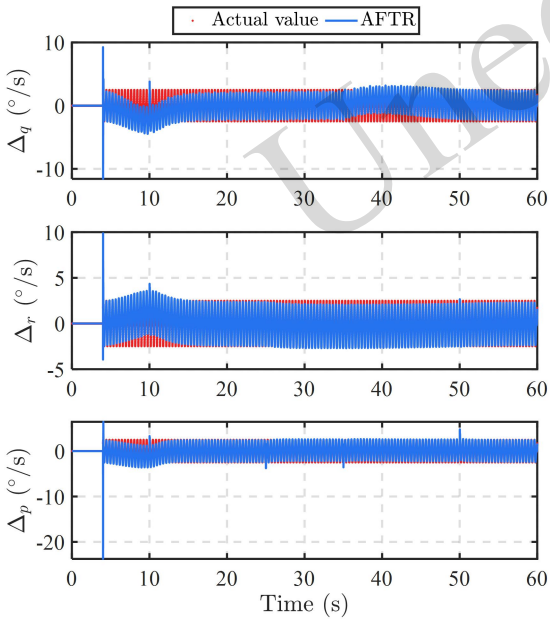

Fig. 5: Disturbance approximation in the angular rate channel.

2) Performance of AFTR: Some time-varying disturbances were introduced into the dynamic model, and then the performance of the designed AFTR was verified.

$$\Delta_\Omega = (0.02\sin(5\pi t) + 0.03\cos(2\pi t)) \cdot [1, 1, 1]^{\mathrm{T}} \quad (24)$$

$$\Delta_\omega = (0.02\sin(10\pi t) + 0.03\cos(5\pi t)) \cdot [1, 1, 1]^{\mathrm{T}} \quad (25)$$

The above disturbance expressions consider that the angular rates may experience perturbation effects at a greater frequency than angle variables. Figs. 4 and 5 show that the external unmatched disturbances within the attitude angle channel and angular rate channel are well estimated by the proposed AFTR observer. The approximation errors of the attitude angle in the three channels shown in Fig. 4 have a maximum of $[2.5264°, 1.2720°, 2.3290°]$ and an average error of $[0.0568°, 0.0432°, 0.0667°]$, which meets the required estimation accuracy throughout the total flight process. Meanwhile, the approximation errors of the attitude angular rates in the three channels in Fig. 5 are $[13.7805°/s, 7.6778°/s, 25.8006°/s]$ at maximum in the transition time node and $[0.4149°/s, 0.1656°/s, 0.1639°/s]$ on average during the stable convergence process. The fluctuations with deviation occur within the first 15 s, which may be caused by additional unknown uncertainties produced by the propagation of estimated errors from the outer-loop to the inner-loop channel. Eventually, these deviations will be eliminated under the fixed-time compensation control.

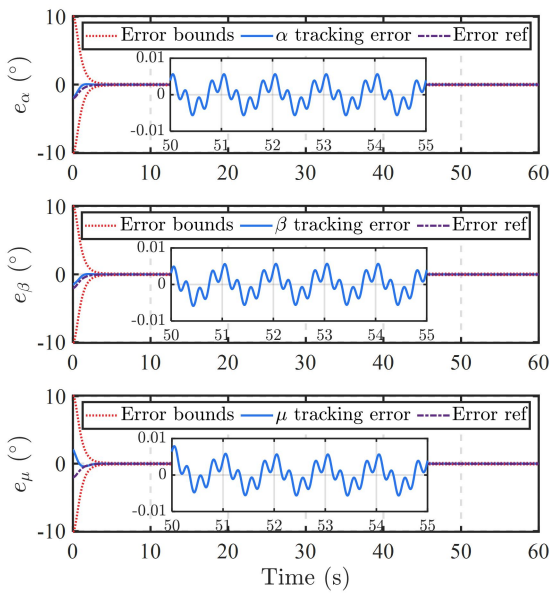

Fig. 6: Tracking errors of the angle with the observer.

3) Integrated Performance Verification with Disturbances and Uncertainties: Taking model uncertainties, aerodynamic and atmospheric parameters, external disturbances from Eqs. (24) and (25) and other perturbation factors into account, Figs. 6 and 7 show that the steady-state errors for both angle and angular rates are all less than 10^{-2} deg with

Unedited

the compensation control of AFTR, which is interrelated to the performance verification in Fig. 3.

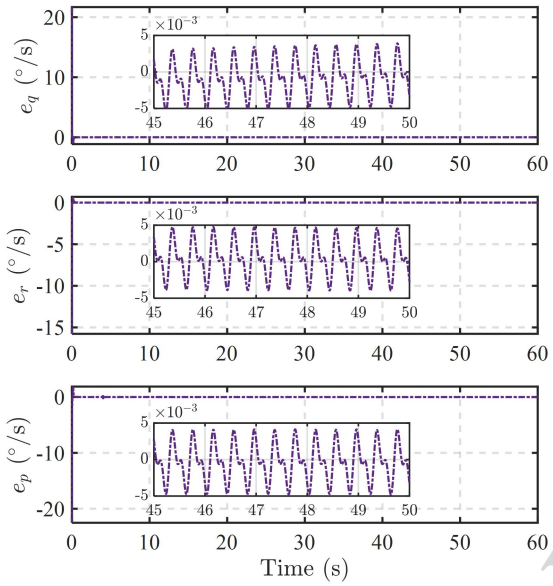

Fig. 7: Tracking errors of the angular rate with the observer.

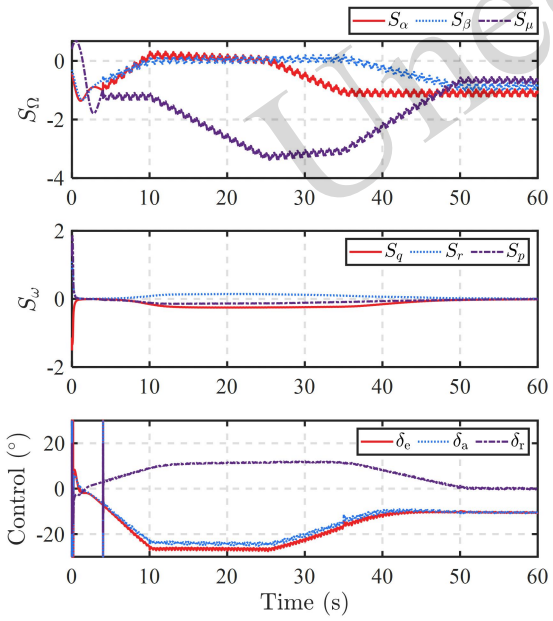

Fig. 8: Sliding mode manifolds and control inputs with observer.

The control inputs in Fig. 8 can rapidly respond to and correct the introduced disturbances and uncertainties, and the sudden change in curves is first reflected in Fig. 5. The reason for this phenomenon is the short-lived intense response of the control system to sudden perturbations. The designed sliding mode manifolds in three channels can achieve effective convergence in fixed time (Fig. 8). Consistency between the convergence trends of the angle sliding mode manifolds and the reference angle signals can be obtained when introducing the continuous smooth reference angle signals and effective controller. The above discussion shows that the designed observer and controller can achieve robust control of a complex attitude system for high-speed aircraft.

4.2. Comparative Case

Excluding the effects of external disturbances while keeping the parameter uncertainties, in this section we describe a comparative analysis among the proposed controller, the finite-time controller, the fuzzy fixed-time sliding mode controller of Chen et al. (2023) denoted as Ref[A], and the proportional-integral (PI) controller of Bu et al. (2023) denoted as Ref[B]. The comparative results are shown in Figs. 9-15. The angle error profiles in Fig. 9 and actual angle tracking profiles in Fig. 10 show that the proposed controller can achieve more precise convergence than the other three methods, characterized by the absence of overshooting and severe oscillations. Similarly, the tracking errors of angular rates in Fig. 11 and the actual signal tracking trajectories in Fig. 12 show stable and excellent results under the funnel-guided fixed-time sliding mode scheme. Defining the average control energy as $E_i = \left(\sum_{t=0}^{60} u_i(t)/60\right)^2$, $i = 1,2,3$, where i represents the angle channel then, from radar figures presented in Figs. 13-15, the control performance of the proposed method in the three channels was better than that of the other three methods in respect of settling time, steady-state accuracy and average control energy, which intuitively reflect faster error convergence and higher tracking accuracy with less energy loss.

Unedited

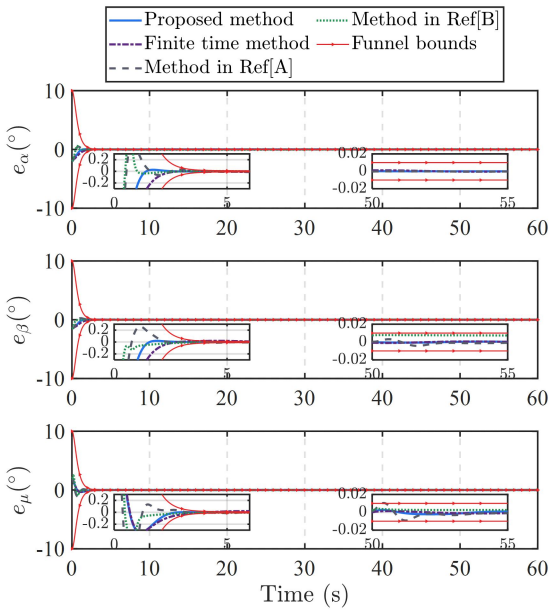

Fig. 9: Tracking errors and bounds of attitude angles of the proposed method compared with those of another three methods.

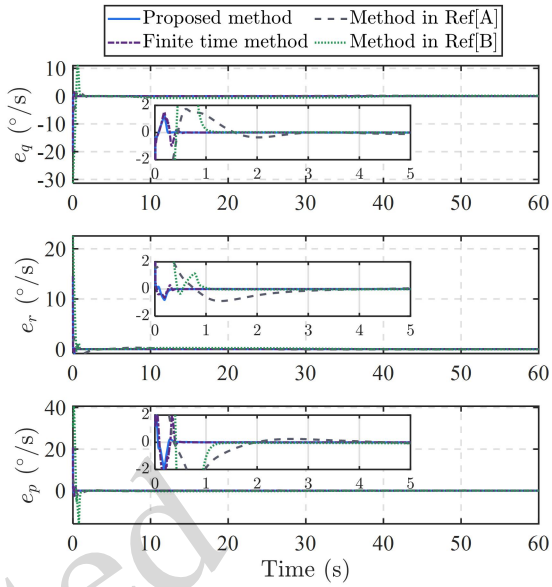

Fig. 11: Tracking errors and bounds of angular rates of the proposed method compared with those of another three methods.

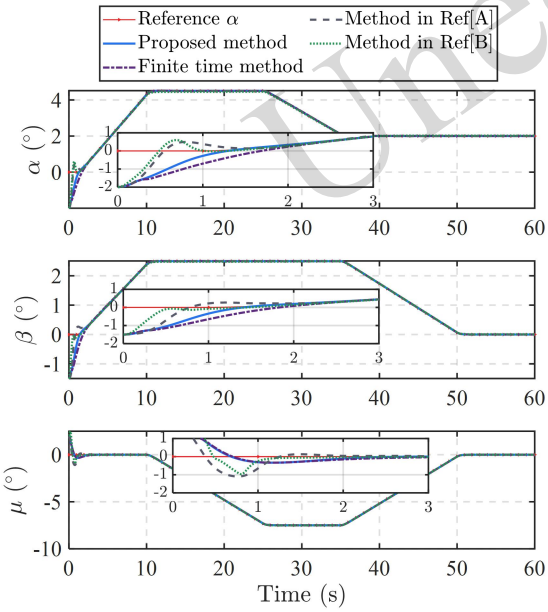

Fig. 10: Tracking trajectories of attitude angles of the proposed method compared those of another three methods.

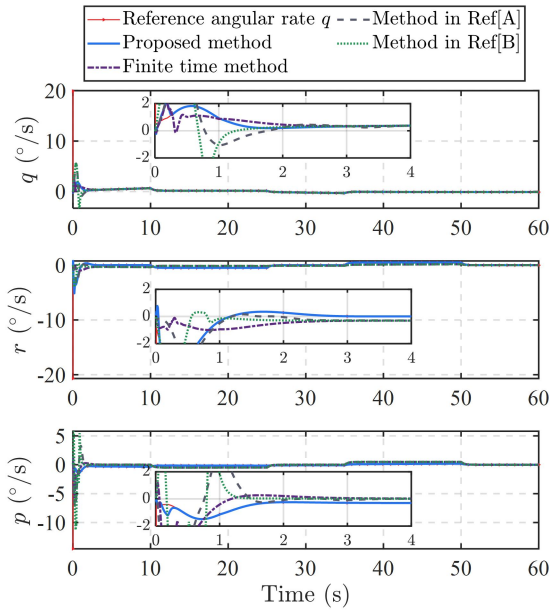

Fig. 12: Tracking trajectories of angular rates of the proposed method compared with those of another three methods.

Unedited

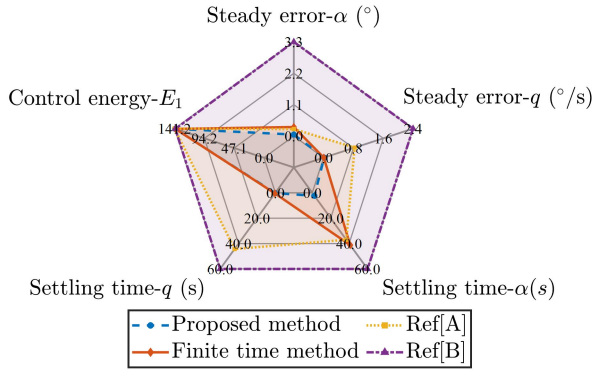

Fig. 13: Radar figure comparing the control performance of the α and q rates in the pitch channel, including total control energy, steady-state error and settling time.

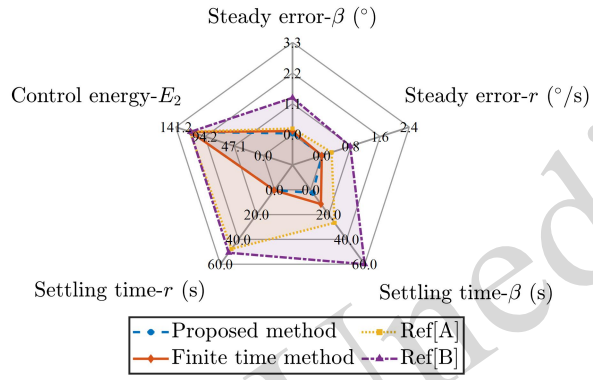

Fig. 14: Radar figure comparing the control performance of the β and r rates in the yaw channel, including total control energy, steady-state error and settling time.

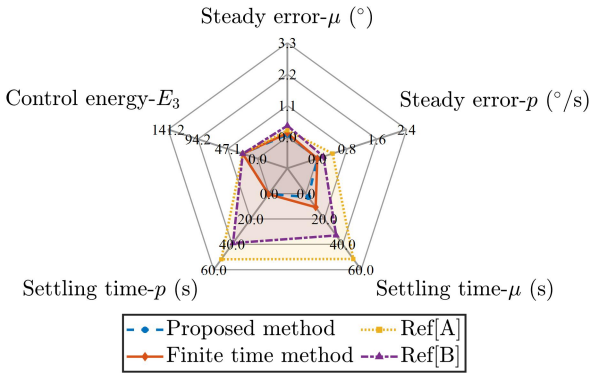

Fig. 15: Radar figure comparing the control performance of the μ and p rates in the roll channel, including settling time (unit s), and steady-state accuracy.

5 Conclusions

In this article, we presented a funnel-guided performance-prescribed robust fixed-time attitude control framework with an AFTR observer for high-speed aircraft. An adaptive parameter-updating AFTR observer was first constructed based on second-order error dynamics to perceive the control system's real-time variation. Then we considered an effective funnel function and error convergence strategy for controllable transition and steady-state performance. To ensure the robustness and rapidity of the entire closed-loop flight control system, we propose a double-integral fixed-time sliding mode control scheme and an oscillation-suppression skill by a designed auxiliary function during the convergence stage. The resulting simulation findings suggest that the control performance desired for high-speed aircraft can be achieved in the presence of unknown uncertainties. Overall, the composite control scheme proposed in this paper can accomplish attitude control tasks for high-speed aircraft under strong nonlinearity and complex coupling with remarkable steady-state error and a robust convergence process. Based on the similarities in system modeling approaches and the empirical guidelines for parameter fine-tuning, the proposed composite controller can also be effectively applied to tracking control tasks in other nonlinear systems.

Unedited

Acknowledgments

This work was supported by the National Natural Science Foundation of China (No. 11972368) and the Natural Science Foundation of Hunan Province (No. 2021JJ10045), China.

Author contributions

Kai AN, designed the research, processed the corresponding data and wrote the first draft of the manuscript. Wei HUANG and Shuang-xi LIU helped organize the manuscript. Kai AN and Wei HUANG revised and edited the final version.

Conflict of interest

Kai AN, Wei HUANG, Shuang-xi LIU declare that they have no conflict of interest.

References

An K, Guo ZY, Huang W, et al., 2022. Leap trajectory tracking control based on sliding mode theory for hypersonic gliding vehicle. *Journal of Zhejiang University-SCIENCE A*, 23, 188-207. https://doi.org/10.1631/jzus.A2100362.

Bao CY, Wang P, Tang GJ, 2023. Data-driven based model-free adaptive optimal control method for hypersonic morphing vehicle. *IEEE Transactions on*

Aerospace and Electronic Systems, 59(4), 3713-3725. https://doi.org/10.1109/TAES.2022.3230633.

Bechlioulis CP, Rovithakis GA, 2008. Robust adaptive control of feedback linearizable MIMO nonlinear systems with prescribed performance. *IEEE Transactions on Automatic Control*, 53(9), 2090-2099. https://doi.org/10.1109/TAC.2008.929402.

Berger T, Rauert AL, 2020. Funnel cruise control. *Automatica*, 119, 109061. https://doi.org/10.1016/j.automatica.2020.109061.

Bouaiss O, Mechgoug R, Taleb-Ahmed A, et al., 2024. Robust trajectory tracking of quadrotors using adaptive radial basis function network compensation control. *Journal of the Franklin Institute*, 361(3), 1167-1185. https://doi.org/10.1016/j.jfranklin.2023.12.045.

Bu X, 2023. Prescribed performance control approaches, applications and challenges: A comprehensive survey. *Asian Journal of Control*, 25(1), 241-261. https://doi.org/10.1002/asjc.2765.

Bu X, Hua C, Lv M, et al., 2023. Flight control of waverider vehicles with fragility-avoidance prescribed performance. *IEEE Transactions on Aerospace and Electronic Systems*, 59(5), 5248-5261. https://doi.org/10.1109/TAES.2023.3251314.

Bu X, Xiao Y, 2018. Prescribed performance-based low-computational cost fuzzy control of a hypersonic vehicle using non-affine models. *Advances in Mechanical Engineering*, 10(2), 1-12. https://doi.org/10.1177/1687814018757261.

Chen H, Wang P, Tang GJ, 2023. Fuzzy disturbance observer-based fixed-time sliding mode control for hypersonic morphing vehicles with uncertainties. *IEEE Transactions on Aerospace and Electronic Systems,* 59(4), 3521-3530. https://doi.org/10.1109/TAES.2022.3227886.

Chen L, Liu Z, Dang Q, et al., 2024. Robust fixed-time flight controller for a dual-system convertible UAV in the cruise mode. *Defence Technology*, 39, 53-66. https://doi.org/10.1016/j.dt.2024.04.009.

Chen M, Wang H, Liu X, 2021. Adaptive fuzzy practical fixed-time tracking control of nonlinear systems. *IEEE Transactions on Fuzzy Systems*, 29(3), 664-673. https://doi.org/10.1109/TFUZZ.2019.2959972.

Ding Y, Yue X, Liu C, et al., 2022. Finite-time controller design with adaptive fixed-time anti-saturation compensator for hypersonic vehicle. *ISA Transactions*, 122, 96-113. https://doi.org/10.1016/j.isatra.2021.04.038.

Dong Z, Li Y, Lv M, et al., 2022. Fuzzy adaptive prescribed performance fault-tolerant control for HFVs with fixed-time convergence guarantee. *International Journal of Aerospace Engineering*, 2022, 1-17. https://doi.org/10.1155/2022/2438657.

Guo Y, Xu B, 2022. Finite-time deterministic learning command filtered control for hypersonic flight vehicle. *IEEE Transactions on Aerospace and Electronic Systems*, 58(5), 4214-4225. https://doi.org/10.1109/TAES.2022.3160687.

Kashmiri S, Mirmirani M, Colgren R, 2012. Six-DOF modeling and simulation of a generic hypersonic vehicle for conceptual design studies, AIAA Modeling and Simulation Technologies Conference and Exhibit, p.1-12. https://doi.org/10.2514/6.2004-4805.

Li C, Wang W, Liu Z, et al., 2024. Adaptive neural network based fixed- time attitude tracking control of spacecraft considering input saturation. *Aerospace Science and Technology*, 155, 109746. https://doi.org/10.1016/j.ast.2024.109746.

Li W, Zhao J, Su S, et al., 2023. Adaptive output feedback attitude control for reusable launch vehicle with input constraints and actuator faults. *Aerospace Science and Technology*, 142, 108616. https://doi.org/10.1016/j.ast.2023.108616.

Liu S, Yan J, Cao J, et al., 2021. Review of the precise orbit determination for chinese lunar exploration projects. *Earth and Space Science,* 8, e2020EA001361. https://doi.org/10.1029/2020EA001361.

Lun Y, Wang H, Wu T, et al., 2024. A changeable boundary prescribed performance control for the altitude ground test facility. *Nonlinear Dynamics*, 112(6), 4483-4506. https://doi.org/10.1007/s11071-023-09270-4.

Meng Y, Yu X, Zhu Y, et al., 2024. Fixed-time attitude control of reusable launch vehicles utilizing reliability-based control allocation. *Control Engineering Practice*, 151, 106013. https://doi.org/10.1016/j.conengprac.2024.106013.

Moulay E, Lechappe V, Bernoua E, et al., 2022. Fixed-time sliding mode control with mismatched disturbances. *Automatica*, 136, 110009. https://doi.org/10.1016/j.automatica.2021.110009.

Parsegov S, Polyakov A, Shcherbakov P, 2012. Nonlinear fixed- time control protocol for uniform allocation of agents on a segment, IEEE 51st Annual Conference on Decision and Control (CDC), p.7732-7737. https://doi.org/10.1109/CDC.2012.6426570.

Polyakov A, 2012. Nonlinear feedback design for fixed-time stabilization of linear control systems. *IEEE Transactions on Automatic Control*, 57(8), 2106-2110. https://doi.org/10.1109/TAC.2011.2179869.

Qian C. Lin W, 2001. Non-Lipschitz continuous stabilizers for nonlinear systems with uncontrollable unstable linearization. *Systems & Control Letters*, 42(3), 185-200. https://doi.org/10.1016/S0167-6911(00)00089-X.

Shao Y, Jin Y, Huang Z, et al., 2024. Finite-time path following control of a sailboat with actuator failure and unknown sideslip angle. *Journal of Zhejiang University-SCIENCE A*, 25(9), 443-454. https://doi.org/10.1631/jzus.A2300184.

Shen Y, Zhou D, Wu Y, et al., 2023. Anti-disturbance control for HVs system subject to nonlinear actuator characteristics with extended state observer. *Journal of the Franklin Institute*, 360, 14676-14695.

Unedited

https://doi.org/10.1016/j.jfranklin.2023.10.005.
Song JG, Zhang JX, 2024. Fault-tolerant prescribed performance control of nonlinear systems with process faults and actuator failures. *ISA Transactions*, 144, 220-227. https://doi.org/10.1016/j.isatra.2023.11.010.
Sun J, Yi J, Pu Z, et al., 2020. Fixed-time sliding mode disturbance observer-based non-smooth backstepping control for hypersonic vehicles. *IEEE Transactions on Systems, Man, and Cybernetics: Systems*, 50(11), 4377-4386. https://doi.org/10.1109/TSMC.2018.2847706.
Tan J, Guo S, 2022. Backstepping control with fixed-time prescribed performance for fixed wing UAV under model uncertainties and external disturbances. *International Journal of Control*, 95, 934-951. https://doi.org/10.1080/00207179.2020.1831700.
Wang F, Zhou C, Hua C, 2024. Adaptive predefined time neural filtered control design for an uncertain nonlinear system and application to flight control. *Applied Mathematical Modelling*, 129, 25-47. https://doi.org/10.1016/j.apm.2024.01.044.
Wang G, Xia H, 2024. Fault-tolerant learning control of air-breathing hypersonic vehicles with uncertain parameters and actuator faults. *Expert Systems with Applications*, 238, 121874. https://doi.org/10.1016/j.eswa.2023.121874.
Wang Y, Hu J, 2018. Improved prescribed performance control for air-breathing hypersonic vehicles with unknown deadzone input nonlinearity. *ISA Transactions*, 79, 95-107. https://doi.org/10.1016/j.isatra.2018.05.008.
Wu T, Wang H, Yu Y, et al., 2021. Quantized fixed-time fault-tolerant attitude control for hypersonic reentry vehicles. *Applied Mathematical Modelling*, 98, 143-160. https://doi.org/10.1016/j.apm.2021.04.033.
Xin B, Cheng S, Wang Q, et al., 2023. Fixed-time prescribed performance consensus control for multiagent systems with non-affine faults. *IEEE Transactions on Fuzzy Systems*, 31(10), 3433-3446. https://doi.org/10.1109/TFUZZ.2023.3255889.
Xu S, Guan Y, Wei C, et al., 2022. Reinforcement learning-based tracking control with fixed-time prescribed performance for reusable launch vehicle under input constraints. *Applied Sciences*, 12(15), 7436. https://doi.org/10.3390/app12157436.
Yin Z, Wang B, Xiong R, et al., 2024. Attitude tracking control of hypersonic vehicle based on an improved prescribed performance dynamic surface control. *The Aeronautical Journal*, 128(1323), 875-895. https://doi.org/10.1017/aer.2023.79.
Zhang B, Liang Y, Rao S, et al., 2024. RBFNN-based anti-input saturation control for hypersonic vehicles. *Aerospace*, 11(2), 108. https://doi.org/10.3390/aerospace11020108.
Zhang H, Wang P, Tang, GJ, et al., 2023. Fixed-time sliding mode control for hypersonic morphing vehicles via event-triggering mechanism. *Aerospace Science and Technology*, 140, 108458. https://doi.org/10.1016/j.ast.2023.108458.
Zhang H, Wang P, Tang GJ, et al., 2024. Disturbance observer-based fixed-time control for hypersonic morphing vehicles with uncertainties. *The Aeronautical Journal*, 1326, 1-31. https://doi.org/10.1017/aer.2023.116.
Zhao HW, Yang LB, 2022. Global adaptive neural backstepping control of a flexible hypersonic vehicle with disturbance estimation. *Aircraft Engineering and Aerospace Technology*, 94(4), 492- 504. https://doi.org/10.1108/AEAT-08-2020-0178.
Zhao J, Feng D, Cui J, et al., 2022. Finite-time extended state observer-based fixed-time attitude control for hypersonic vehicles. Mathematics, 10(17), 3162. https://doi.org/10.3390/math10173162.
Zhao S, Wang J, Xu H, et al., 2023. ADP-based attitude-tracking control with prescribed performance for hypersonic vehicles. *IEEE* Transactions *on Aerospace and Electronic Systems*, 59(5), 6419-6431. https://doi.org/10.1109/TAES.2023.3276729.
Zhao S, Wang J, Xu H, et al., 2023. Composite observer-based optimal attitude-tracking control with reinforcement learning for hypersonic vehicles. *IEEE Transactions on Cybernetics*, 53(2), 913-926. https://doi.org/10.1109/TCYB.2022.3192871.
Zuo Z, 2015. Nonsingular fixed-time consensus tracking for second-order multi-agent networks. *Automatica*, 54, 305-309. https://doi.org/10.1016/j.automatica.2015.01.021.
Zuo Z, Tie L, 2014. A new class of finite-time nonlinear consensus protocols for multi-agent systems. *International Journal of Control*, 87(2), 363-370. https://doi.org/10.1080/00207179.2013.834484.

Electronic supplementary materials

Section S2.2, Section S3.1, Section S3.2, Section S3.3, Section S3.4

中文概要

题　目：高速飞行器固定时间鲁棒姿态跟踪控制：一种精确的漏斗引导方法

作　者：安凯，黄伟，刘双喜

机　构：国防科技大学，先进推进技术实验室，中国长沙，410073

目　的：高速飞行器姿态控制系统具有复杂非线性动态耦合特性，飞行过程持续受到环境不确定因素影响，亟需提升对信号的响应速度、精度及

Unedited

抗干扰能力。本文旨在通过结合预设性能方法、滑模理论及 RBFNN 等技术的优势，发展具有严格动态性能约束的鲁棒固定时间姿态控制方案，实现快速且精准的跟踪误差控制。

创新点： 1. 提出一种改进漏斗剖面引导的 PPC 方案；2. 提出融合辅助振荡抑制函数的双环积分固定时间滑模控制器；3. 提出自适应网络权值更新的固定时间 RBFNN 观测器。

方　法： 1. 通过姿态动力学模型，设计自适应固定时间 RBFNN 观测器作为补偿控制；2. 通过转换的误差控制模型，提出漏斗引导的预设性能转换方法，基于此，结合设计的辅助振荡抑制函数，推导出双积分固定时间滑模控制器；3. 通过李雅普诺夫理论证明整个闭环系统的固定时间稳定性；4. 通过标称与对比工况仿真，验证所提姿态集成控制框架的有效性与可靠性。

结　论： 1. 姿态角度与角速度跟踪误差的固定时间收敛特性得到验证，无显著超调与震荡出现；2. 雷达图显示所提方法在调节时间、稳态精度及平均控制能量等方面均有显著优势；3. 融合固定时间收敛特性的 RBFNN 观测器对姿态集成控制框架中的干扰因素具有良好估计。

关键词： 漏斗控制；固定时间理论；姿态控制；RBFNN；高速飞行器

Unedited